Thermoelectric properties and low-temperature transport anomalies in the *p*-type full-Heusler compounds $Fe_{2-x}Cr_xVAl$

N. Reumann,[1,*] A. Riss,[1] F. Garmroudi,[1] M. Parzer,[1] J. Kovacevic,[1] T. Mori,[2,3] and E. Bauer[1]

[1]*Institute of Solid State Physics, Technische Universität Wien, Vienna 1040, Austria*

[2]*International Center for Materials Nanoarchitectonics (WPI-MANA), National Institute for Materials Science, Tsukuba 305-0044, Japan*

[3]*Graduate School of Pure and Applied Sciences, University of Tsukuba, Tsukuba 305-8571, Japan*

(Received 19 July 2022; revised 10 November 2022; accepted 16 November 2022; published 19 December 2022)

Elemental substitutions are successfully used for the optimization of thermoelectric properties of a specific material; it requires, however, a deep understanding of its impact. For this purpose, based on the full-Heusler material Fe_2VAl, various compounds ($Fe_{2-x}Cr_xVAl$) were synthesized by substituting Cr for Fe in a wide range from $x = 0.005$ up to $x = 0.4$. X-ray diffraction analysis revealed full solubility of Cr for all concentrations. Bulk thermoelectric properties, such as electrical resistivity, Seebeck coefficient, thermal conductivity, and Hall resistivity were measured from 2 K up to 780 K, and all results were discussed in the context of the outcome of density functional calculations. Transport anomalies, resembling Kondo scattering, were observed for all samples below 30 K. Finally, an increased effective number of valence electrons of 7 for Cr was phenomenologically determined, which revealed good agreement with other *p*-type doping studies of Fe_2VAl.

DOI: 10.1103/PhysRevB.106.235138

I. INTRODUCTION

The research on thermoelectric devices, whether on waste heat harvesting, cooling, or other applications has seen great advancements in the past decades [1–3]. For such devices a reasonably large thermoelectric figure of merit $ZT = S^2\sigma T/\kappa$ is the determining factor for most practical applications. S is the Seebeck coefficient, σ the electrical conductivity, T is the absolute temperature, and κ is the total thermal conductivity. Consequently, a solid understanding of the underlying thermoelectric transport mechanisms and how to manipulate them is paramount for the development of thermoelectric devices. Full-Heusler compounds based on Fe_2VAl have recently shown to offer a rich playground for studying and developing new enhancement principles [4,5].

Pristine ternary Fe_2VAl consisting of cheap and abundant elements, is easy to synthesize and has been extensively studied in recent years [6–13]. Both experimental data and density functional theory-(DFT-) based calculations show Fe_2VAl as a semimetal with a small negative indirect band gap as can be seen in Fig. 1. This results in a very low density of states (DOS) at the Fermi energy E_F and a high sensitivity of the transport parameters to doping or elemental substitution. Even though its high-semiconductor-like electrical resistivity, large thermal conductivity, and only moderate Seebeck coefficient are not suitable for thermoelectric application, Fe_2VAl-based compounds with moderate amounts of other substituted elements have shown substantial improvements of all parameters, achieving high power factors $S^2\sigma$ up to 10.3 $\mathrm{mW\,m^{-1}\,K^{-2}}$ for Ta- and Si-based substitutions by band engineering [12]. Although a wide range of elements for *n*-type doping has been studied, research into *p*-type doping is sparse. Additionally, nearly all of these elemental substitutions are based on substituting either V or Al.

Disorder, such as Fe/V antisite occupations, plays a significant role in undoped Fe_2VAl, influencing thermoelectric properties as well as magnetic features [14,15]. For example, both superparamagnetic cluster glass behavior (see Ref. [16]) with an average magnetic moment $\mu \approx 5000\mu_B$ and isolated magnetic impurities arising from Fe/V antisite defects with $\mu = 3.7\mu_B$ have been observed in the otherwise nonmagnetic host matrix of fully ordered Fe_2VAl [17,18].

The present paper aims to provide deeper understanding of *p*-type transport in Fe_2VAl and how it can be utilized to create enhanced thermoelectric materials through band-structure engineering. This will be achieved by quantifying the effect of Fe/Cr substitution on the thermoelectric properties. Moreover, low-temperature transport anomalies are observed, resembling Kondo-like carrier scattering, which is corroborated by electronic structure calculations, indicating that Cr atoms located at the Fe site lead to magnetic impurities.

II. EXPERIMENTAL AND COMPUTATIONAL METHODS

A. Synthesis

For the synthesis of the bulk material, elements of high purity (Fe 99.98%, Cr 99.99%, V 99.93%, Al 99.99%, and Si 99.999%) were weighed in and then melted in a high-frequency induction furnace. This resulted in polycrystalline ingots of around 4 to 5 g with only a marginal mass loss of less than 0.1%. As-cast samples were then annealed at 1073 K for 168 h inside an evacuated ($p \approx 10^{-5}$ mbar) and sealed quartz tube. The annealed ingots were then cut into the appropriate geometry for the respective x-ray and transport measurements using an aluminum oxide cutting wheel.

*reumann.n@hotmail.com

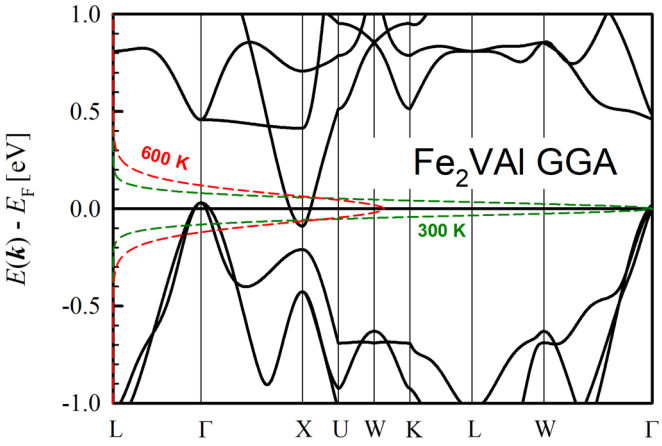

FIG. 1. Electronic band structure of Fe_2VAl around the Fermi energy E_F. Energy derivatives of the Fermi-Dirac distribution at T = 300 and 600 K are indicated as colored dashed lines. Reproduced from Ref. [12].

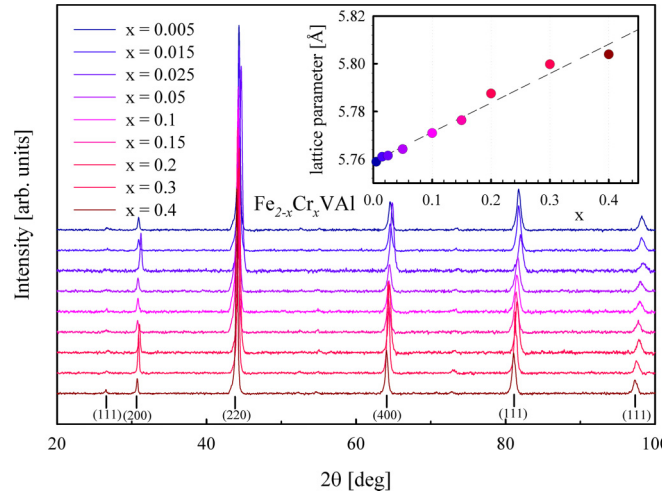

FIG. 2. Powder XRD patterns of $Fe_{2-x}Cr_xVAl$ taken at room temperature for various concentrations of x. The inset shows the lattice parameter of each sample calculated by Rietveld refinement from the corresponding XRD graph, assuming a full-Heusler $L2_1$ crystal structure.

B. X-ray diffraction

To examine the phase purity and the lattice parameters of the polycrystalline $Fe_{2-x}Cr_xVAl$ samples, x-ray diffraction (XRD) measurements were performed on ground samples, and the lattice parameter was determined from Rietveld refinements. Cu $K\alpha$ radiation and a Bragg-Brentano geometry was used (PANalytical XPert Pro MPD).

C. Electronic and thermal transports

The electrical resistivity and Seebeck coefficient above 300 K were simultaneously obtained using a ZEM3-ULVAC device. Seebeck measurements below 300 K were performed separately but on the same sample, utilizing a so-called "seesaw heating" method [19]. For the low-temperature resistivity measurement the Van der Pauw method was used. The low-temperature data were adjusted by a small constant multiplicative factor to fit the standardized high-temperature measurements.

Thermal conductivity was measured in a steady-state heat-flow experimental setup. The measured data were then corrected for radiation loss by fitting the Callaway model [20] with an additional T^3 term as has been successfully performed in previous studies [8,21,22]. To acquire the lattice thermal conductivity the electronic portion was subtracted using the Wiedemann-Franz law with a Lorenz number of $2.44 \times 10^{-8}\ \mathrm{W\,\Omega\,K^{-2}}$.

For the calculation of the Hall mobility and charge-carrier concentration, Hall resistivity at room temperature was measured. The Hall mobility and charge-carrier concentration were then evaluated within a single-band model. Although this seems to be justified by the linear Hall resistivity, it has to be mentioned that due to the semi-metal-like band-structure, contributions from both holelike and electronlike may be relevant. For details of the evaluation of the Hall measurements see the Supplemental Material [23].

D. Density functional theory calculations

DFT calculations of the electronic density of states of $Fe_{2-x}Cr_xVAl$ were carried out. Performing supercell calculations on a 3×3×3 rhombohedral supercell with 108 atoms allowed to investigate the effect of partial Cr substitution where a single Cr atom was replaced for one of the 54 Fe atoms and compared to results of the quaternary FeCrVAl and pristine Fe_2VAl.

III. RESULTS

A. Crystal structure

XRD patterns and the composition-dependent lattice parameters are presented in Fig. 2. It can be seen that all samples, even up to high-Cr concentrations of $x = 0.4$, exhibit the same characteristic full-Heusler structure ($L2_1$) pattern. The linear dependence of the lattice parameter on the Cr concentration also indicates high solubility of Cr and homogeneity of the Heusler phase. Additionally, our DFT-based calculations show the defect-formation enthalpy for a Fe/Cr substitution to be $H_{\mathrm{Fe/Cr}} = -7.83$ eV compared to $H_{\mathrm{V/Cr}} = +0.84$ eV, indicating that Cr occupying the Fe sublattice is more energetically favorable than Cr occupying the V sublattice and V occupying the Fe sublattice. (V_{Fe} antisite: +1.513 eV) [24].

B. Electronic structure

Figure 3 shows the spin-polarized electronic densities of states of $Fe_{2-x}Cr_xVAl$ in the dilute limit of Cr substitution ($x \approx 0.02$) and for the full substitution of one Fe sublattice by Cr, i.e., the quaternary Heusler compound FeCrVAl. The electronic structure of Fe_2VAl was calculated as well and was plotted for comparison (dashed gray lines). The first immediate feature which can be noted upon substituting with Cr is the appearance of narrow impurity states inside the pseudogap. Moreover, the spin degeneracy of these states is removed, meaning that Cr on the Fe site forms a magnetic impurity. Upon increasing Cr substitution the degree of spin polarization increases substantially and leads to a half-metallic-like ground state in FeCrVAl, i.e., one spin channel shows a metal-

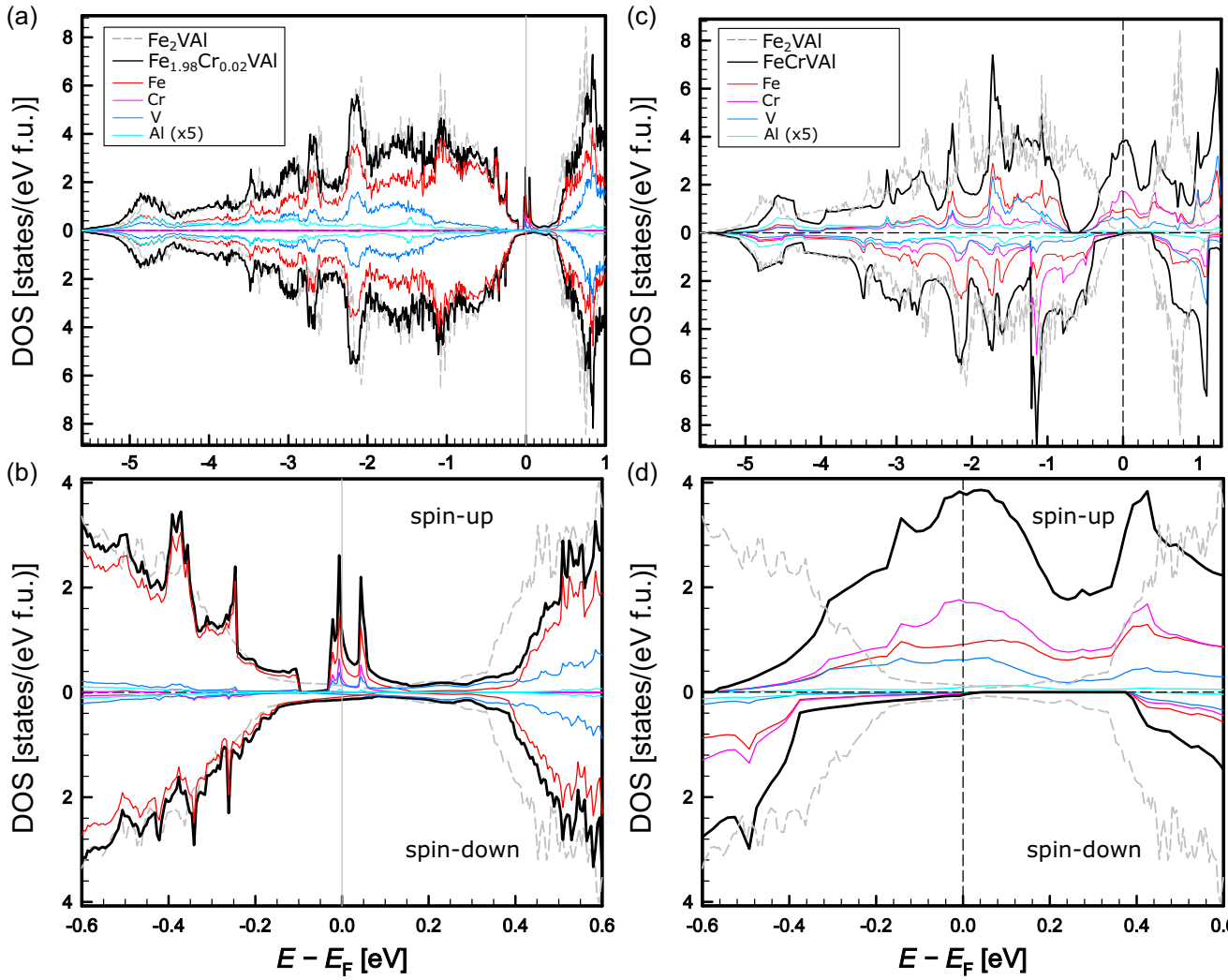

FIG. 3. Energy-dependent DOS of (a) dilute Cr doping of Fe_2VAl ($Fe_{1.98}Cr_{0.02}VAl$) and (b) the fully substituted quaternary compound FeCrVAl. The DOS around the Fermi energy E_F is shown in (b) and (d), respectively.

lic solution, whereas, the minority spin has a band gap at the Fermi energy. By analyzing the partial atom-projected DOS, we find that the majority contribution of electronic states in the impurity band arises from Fe and Cr atoms, followed by V, with very little Al contribution. Interestingly, for the dilute case ($x \approx 0.02$) the main contribution arises from the Fe atoms near the Cr impurity, whereas, for the quaternary Heusler compound, in-gap states have predominant Cr character.

Such a behavior where the contribution of the impurity states mostly stems from the atoms of the host material surrounding the impurity and not the impurity itself has, for example, also been found in other semiconductors, such as thallium-doped PbTe [25]. Thus, it is possible that small amounts of Cr impurities in $Fe_{2-x}Cr_xVAl$ act in a similar manner as a catalyst for the formation of resonantlike states. However, as the amount of Cr impurities increases, the overlap of wave functions will lead to the formation of a real impurity band, which has predominant Cr character. We further point out that the DOS of the minority spin retains its integrity and shows similar features even for the FeCrVAl quaternary Heusler compound.

To summarize, DFT calculations suggest the formation of magnetic impurity states due to Fe/Cr substitution and a half-metallic-like ground state for the quaternary FeCrVAl compound. With increasing Cr substitution the in-gap states become broader around the Fermi level and eventually fill out the entire pseudogap.

C. Electrical resistivity

As shown in Fig. 4, the temperature-dependent electrical resistivity $\rho(T)$ of $Fe_{2-x}Cr_xVAl$ ($0 < x \leqslant 0.4$) shows for all x a semiconductorlike behavior above room temperature due to the activation of charge carriers across the pseudogap. Presumably, this is also the case in undoped Fe_2VAl, which exhibits this behavior across the whole temperature range. For higher concentrations of Cr, the semiconductorlike behavior diminishes as the samples become more and more metal-like below room temperature. Additionally, at very low temperatures, below 30 K, a logarithmic increase in the resistivity was obtained for all samples. These low-temperature anomalies might result from a single-impurity-type Kondo effect due

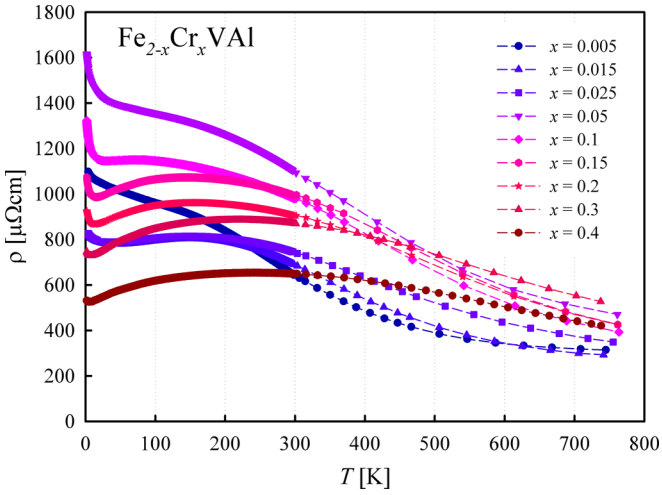

FIG. 4. Temperature-dependent electrical resistivity ρ of $Fe_{2-x}Cr_xVAl$ for various concentrations of x. Dashed lines are added as a visual guide.

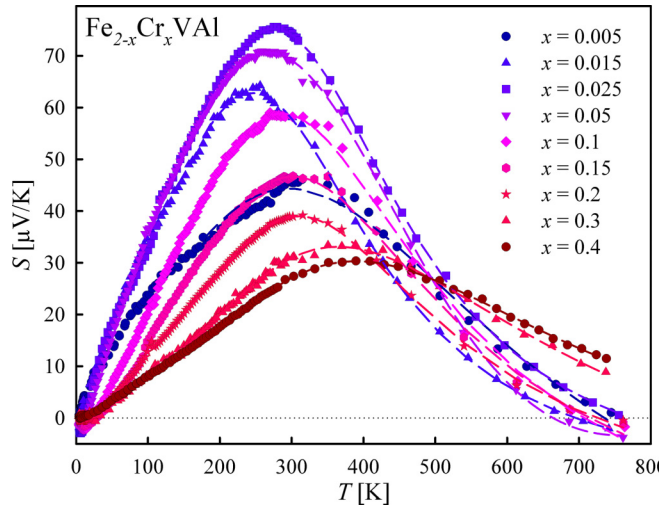

FIG. 5. Temperature-dependent Seebeck coefficient measurements of $Fe_{2-x}Cr_xVAl$ between 4 and 800 K. The dashed lines indicate a parabolic three-band model fit in the temperature range of 100–750 K.

to the interaction of conduction electrons with the almost localized Cr ions and will be further discussed in Secn IV B. The overall change inthe temperature-dependent resistivity for different Cr concentrations can be understood as arising from two competing factors: Cr contributes less electrons and, therefore, lowers the Fermi energy further into the valence band. This increases the charge-carrier concentration and, consequently, decreases the electrical resistivity. The other competing factor is the random potential fluctuation induced by the Cr atoms on the Fe sublattices. This leads to a significant additional impurity scattering since the majority of electronic states in the valence band has Fe orbital character [26]. Moreover, electronic structure calculations suggest that the partial substitution of Cr leads to narrow less dispersive or localized impurity states at the valence-band edge. For small concentrations, such as $x = 0.05$ the additional impurity scattering is dominant whereas for high concentrations, such as $x = 0.4$ the additional charge carriers outweigh the effect of impurity scattering leading to an significantly reduced low-temperature resistivity.

D. Seebeck effect

Measurements of the temperature-dependent Seebeck coefficient $S(T)$ from 4 K up to more than 700 K are shown in Fig. 5. All samples exhibit a maximum between 200 and 400 K with the sample $x = 0.025$ showing the highest value of $S = 75\ \mu$/K.

Qualitatively, the composition-dependent behavior of the maximum Seebeck coefficient for $Fe_{2-x}Cr_xVAl$ with increasing Cr concentration can be explained as follows: The Seebeck coefficient is the sum of all contributions of all bands near the Fermi level with holelike valence bands contributing with a positive sign and electronlike conduction bands, contributing a negative signed thermopower. In the case of Fe_2VAl or at very low concentrations (i.e., $x = 0.005$), both holelike and electronlike carriers contribute significantly, leading to only moderately large values of the Seebeck coefficient. For slightly higher Cr concentrations, the Fermi level drops, and the negative contribution of the conduction band diminishes, which increases the Seebeck coefficient up to Cr concentrations of $x \approx 0.025$. A further decrease in the Fermi level into the valence band increases the DOS at $E = E_F$ and, therefore, decreases the Seebeck coefficient as described by the Mott formula,

$$S \propto \frac{\partial N(E_F)/\partial E}{N(E_F)},$$

with $N(E_F)$ being the DOS at the Fermi energy. This is dominant for high-Cr concentrations and diminishes the resulting Seebeck coefficient, whereas shifting the maximum to higher temperatures due to a loss of bipolar conduction.

Even though these arguments (i.e., a rigid-band-like shift) neglect other effects, such as the formation of a Cr-impurity

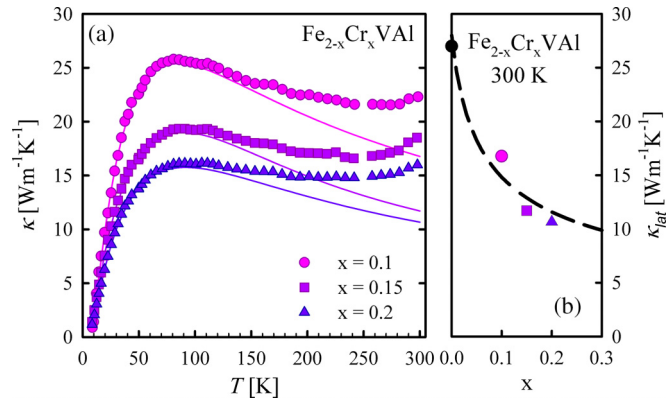

FIG. 6. (a) Temperature-dependent thermal conductivity of a selection of samples of $Fe_{2-x}Cr_xVAl$ from 4 K to room temperature. Data points in (a) represent the total measured thermal conductivity. The solid lines are least-squares fits as explained in the text. (b) Lattice thermal conductivity for various concentrations of Cr at $T =$ 300 K. The dashed line in (b) indicates a Klemens model fit [27]. For comparison an additional data point for undoped Fe_2VAl was added.

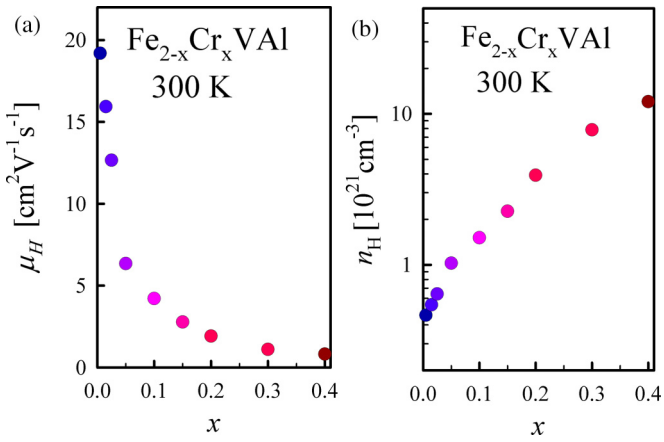

FIG. 7. Cr concentration dependence of the charge-carrier mobility and density calculated from Hall-resistivity measurements at room temperature of $Fe_{2-x}Cr_xVAl$.

band or other changes in the band structure, they can reasonably well explain the observed behavior. These simple arguments are further supported by the dependence of S on the valence electron concentration as shown in Fig. 8 (discussed in Sec. IV A).

Moreover, a three-parabolic-band model as has been employed successfully in similar compounds [8,10,12], was used to fit the Seebeck data (depicted as dashed lines in Fig. 5). Obviously, experimental data above about 50 K are well accounted for by this model, revealing reasonable facts and figures regarding the respective valence and conduction bands (details are collected in the Supplemental Material [23]). Below about 50 K, the three-parabolic-band model predicts an almost linear dependence of $S(T)$; experimental data, however, deviate from this linearity because of the presence of Kondo interactions. (details on the fit parameters can be found in Supplemental Material [23]).

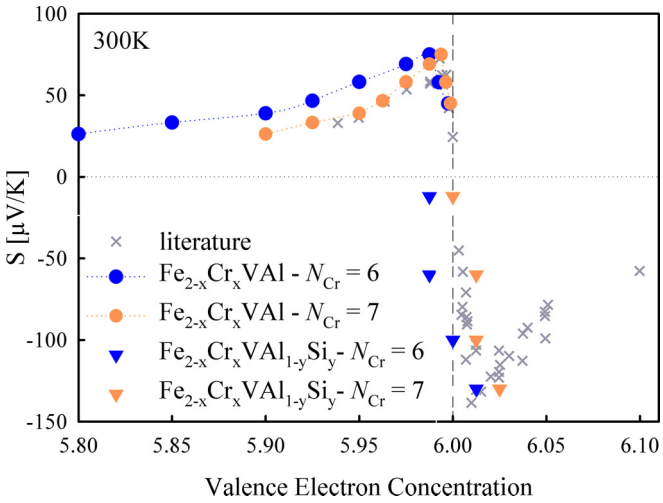

FIG. 8. Valence electron concentration dependency of the Seebeck coefficient shown for $Fe_{2-x}Cr_xVAl$ and $Fe_{2-x}Cr_xVAl_{1-y}Si_y$. Although an effective valence electron count N_{Cr} of 6 for Cr is conventionally expected, a count of 7 fits very well with data from other doping studies on Fe_2VAl [9,11,29–40].

E. Thermal conductivity

The temperature-dependent thermal conductivity κ was measured for representative samples with Cr concentrations $x = 0.1$, $x = 0.15$, and $x = 0.2$. Results are as depicted in Figs. 6(a) and 6(b). The lattice thermal conductivity (solid lines in Fig. 6) was calculated by fitting a Callaway model [20] with an additional T^3 radiation loss term and subtracting the electronic contribution, which was calculated using the Wiedemann-Franz law.

In Fig. 6(b), the Cr concentration dependence of the lattice contribution κ_{lat} shows a decrease due to point defect scattering of phonons by mass and strain field fluctuations. The decrease in κ_{lat} with composition is found to be comparable to n-type $Fe_2VAl_{1-x}Si_x$-based Heusler compounds [9]. Qualitatively, the composition-dependent behavior can be well described employing the Klemens model [27] as shown in Fig. 6(b). Within this model the ratio of the thermal conductivity of a defective solid κ_d to that of the pure solid κ_0 is given by

$$\frac{\kappa_d}{\kappa_0} = \frac{\tan^{-1} u}{u} \quad \text{and} \quad u^2 = \frac{\left(6\pi^5 V_0^2\right)^{1/3}}{2k_B v_s}\kappa_0 \Gamma,$$

where V_0 is the volume per atom, v_s the speed of sound, and Γ is the point defect scattering parameter which is related to the defect concentration by $\Gamma \propto x(1-x)$ [28].

F. Mobility and charge-carrier concentration

The calculated charge-carrier mobility and charge-carrier concentrations from Hall measurements (see the Supplemental Material [23]) at $T = 300$ K can be seen in Fig. 7. The concentration dependence of the mobility shows a dramatic decrease and is more than one order of magnitude smaller for $x = 0.4$. This arises from increased carrier scattering on the randomly distributed Cr ions on the Fe sublattices. The increase in the charge-carrier concentration is consistent with the experimental results of the Seebeck coefficient and indicates a shift of the Fermi energy deeper into the valence band.

IV. DISCUSSION

A. Prospects of band-structure engineering by Fe/Cr substitution

The concept of band-structure engineering follows the intentional modification of both the shape of the band structure near the Fermi level and the position of the Fermi level itself, to achieve intended changes in the physical properties. This is usually accomplished by elemental substitution or changes in the synthesis method. For this purpose, it is necessary to understand and be able to predict the effect of specific elemental substitutions on the pristine material.

To quantify and compare the results of different elemental substitutions, the Seebeck coefficient of various Fe_2VAl-based compounds is plotted as a function of the valence electron concentration. Results are shown in Fig. 8. Assuming a rigid band structure, a change in the valence electron concentration (VEC) is phenomenologically comparable with a change in the Fermi level and is remarkably consistent for various Fe_2VAl-based compounds (see examples from literature in

Fig. 8). The VEC is commonly calculated by averaging over the valence electron count N of all constituent elements. In case of Fe_2VAl (N_{Fe}: 8, N_V: 5, and N_{Al}: 3), this leads to VEC = 6. Although this simple counting of valence electrons works for many elemental substitutions in Fe_2VAl, it seems to be different for Cr with a formal valence electron count $N_{Cr} = 6$ when substituted on the Fe site in the Fe_2VAl structure (see Fig. 8) which indicates significant changes in the electronic structure.

When, however, considering $N_{Cr} = 7$, the overall behavior of the elemental substitution is in very good agreement with all other substitutions and is reminiscent of a rigid-band-like shift in the Fermi energy. Although this observation is of pure phenomenological nature and does not have any direct physical meaning, it is crucial when tuning the Fermi level for optimal thermoelectric performance. To corroborate this finding, several $Fe_{2-x}Cr_xVAl_{1-y}Si_y$-based samples were synthesized in a second batch, and their respective Seebeck coefficient at $T = 300$ K was measured. Here, cosubstitution of Al/Si is used as an n-type doping agent to increase both the total valence electron concentration and the position of the Fermi level, see Fig. 8. It can be seen that, in accordance with previous arguments, these samples also show better consistency with previous doping studies when assuming $N_{Cr} = 7$ instead of 6. Again, it has to be reiterated that this observation does not imply a true rigid-band-like behavior as it is most likely the case in pure Al/Si substitution but is only of phenomenological nature. For further details on these substitutions see the Supplemental Material [23].

Additionally, the high solubility of Cr is crucial because it facilitates the reduction of the lattice thermal conductivity due to increased crystallographic disorder.

In conclusion, Cr as an elemental substitution for Fe is a useful and predictable tool in the careful crafting of Fe_2VAl-based compounds optimized for thermoelectrical applications.

B. Low-temperature transport anomalies

Both the Seebeck coefficient and the electrical resistivity of $Fe_{2-x}Cr_xVAl$ exhibit a peculiar temperature-dependent behavior below $T \approx 30$ K. In the case of the electrical resistivity, a logarithmic temperature dependence $\rho(T) \propto -\ln(T)$ arises. This can best be observed for $Fe_{1.9}Cr_{0.1}VAl$ (Fig. 9) but is present in each other sample as well.

A peculiar low-temperature anomaly is also observable for the temperature-dependent Seebeck coefficient below 30 K (see Fig. 10). The emergent minimum in $S(T)$ is most pronounced for moderately doped samples, such as $Fe_{1.9}Cr_{0.1}VAl$. For lower concentrations, the $S(T)$ minimum occurs at lower temperatures. For higher concentrations, on the other hand, the low-temperature anomaly becomes suppressed and even vanishes for x approaching 0.4. Together with the anomalous increase in the low-temperature resistivity, this hints to more complex energy-dependent scattering mechanisms.

A possible explanation for both these phenomena can be given by isolated magnetic impurity scattering, i.e., the Kondo effect [41]. Here, a logarithmic energy dependence of the relaxation time $\tau(E) \propto \ln(1/E)$ arises from intermediate spin-flip scattering between the magnetic impurity and the conduction electron spins, resulting in a negative logarithmic $\rho(T)$ dependence (see Fig. 9). Such Kondo-type scattering has previously also been suggested in other substituted Fe_2VAl-based compounds [32].

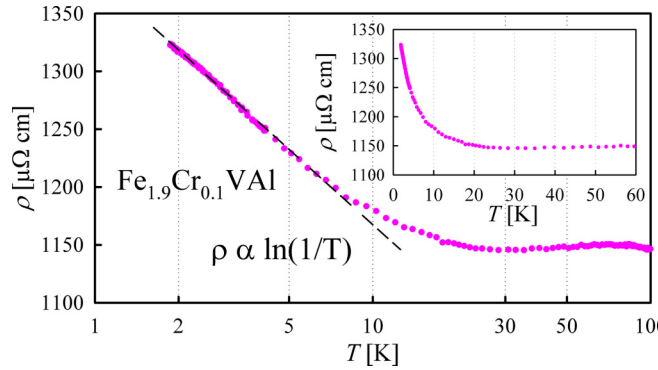

FIG. 9. Temperature-dependent electrical conductivity measurement of $Fe_{1.9}Cr_{0.1}VAl$. The dashed line illustrates the logarithmic temperature dependency at low temperatures. The inset shows the same sample in a linear temperature dependence.

With respect to the Seebeck effect, S (and in absence of any other interaction mechanisms), a universal behavior [42] of $S(T)$ can be expected, revealing a smooth maximum/minimum around the characteristic Kondo temperature T_K. In this scenario, large thermopower values can be obtained as a consequence of an asymmetric relaxation time $\tau(E)$ due to the Kondo resonance around the Fermi energy E_F. Studies of $3d$ magnetic impurities dissolved in a nonmagnetic host, such as Cu or Au revealed pronounced extrema (about |10–20| μV/K) [43]. Diluted chromium in Cu was reported to exhibit a negative thermopower anomaly at low temperatures [44]. In fact, depending on the Cr concentration in $Fe_{2-x}Cr_xVAl$, more or less pronounced minima in $S(T)$ are obvious at low temperatures from Fig. 10.

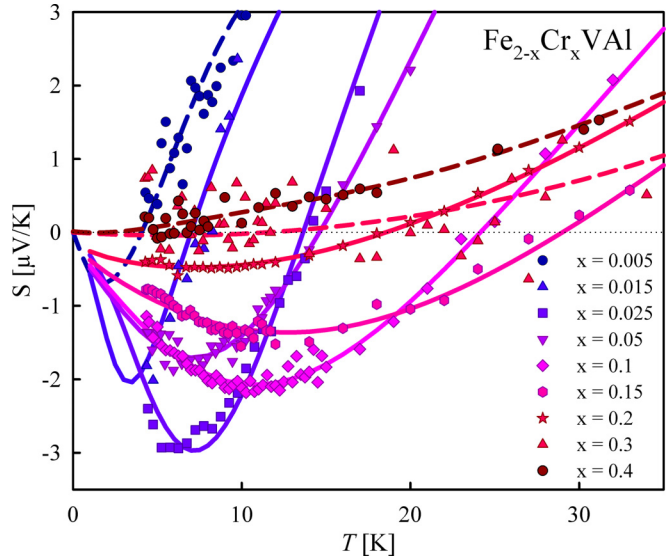

FIG. 10. Low-temperature Seebeck coefficient for $Fe_{2-x}Cr_xVAl$. Solid lines indicate a qualitative Kondo-model fit. Dashed lines indicate simple polynomial fits for visual clarity.

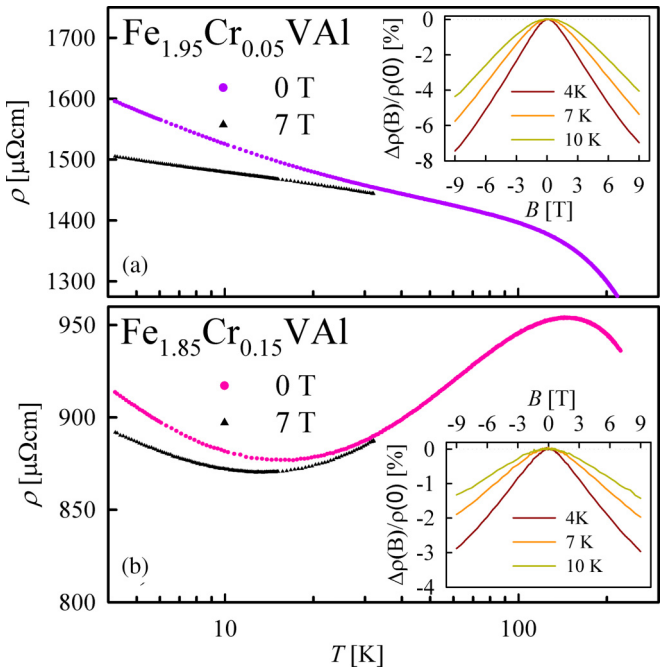

FIG. 11. Temperature-dependent electrical resistivity ρ of (a) $Fe_{1.95}Cr_{0.05}VAl$ and (b) $Fe_{1.85}Cr_{0.15}VAl$ for external fields of 0 and 7 T. The insets show the field-dependent magnetoresistance for various temperatures.

To quantitatively account for this Kondo contribution to $S(T)$, a theory developed by Fischer [45], based on the Heisenberg Hamiltonian, can be utilized. In this model, the Kondo contribution to the Seebeck effect is given by

$$S_{\mathrm{Kondo}}(T) = \frac{\pi^2 J(J+1)\sin(2\alpha)}{[\ln^2(T_{\mathrm{K}}/T) + \pi^2 J(J+1)]^{3/2}},$$

where J is the effective spin moment, α is the scattering phase shift, and T_{K} is the Kondo temperature [46]. Thus, the total Seebeck coefficient is then given by

$$S_{\mathrm{total}}(T) = cS_{\mathrm{Kondo}}(T) + \gamma T,$$

where c is a parameter, depending on the electrical resisitivity and γ is the conventional linear diffusion term at low temperatures. The value of γ was obtained by interpolating the linear temperature dependence significantly above the Kondo contribution. Least-squares fits of $S_{\mathrm{total}}(T)$ to the experimental data reveal good agreement (solid lines, Fig. 10), thus, confirming to some extent the Kondo scenario proposed. Parameters and further details on the fitting procedure can be found in the Supplemental Material [23].

To further investigate the low-temperature transport anomalies, magnetotransport measurements have been performed at low temperatures. In the presence of an external magnetic field Kondo scattering diminishes due to the degeneracy of the intermediate spin-flip state being lifted. As a result, the electrical resistivity is decreased, and the Kondo effect becomes entirely suppressed if the magnetic-field energy corresponds with the Kondo energy $k_{\mathrm{B}}T_{\mathrm{K}}$. Indeed, as can be seen in Fig. 11, the upturn of ρ at low temperatures is significantly suppressed in an external magnetic field. Both insets of Fig. 11 exhibit the magnetoresistance $\Delta\rho/\rho$ at various low temperatures. In accordance to the results of the main panels of Fig. 11, $\Delta\rho/\rho$ is negative, and the field dependence matches a typical Kondo scenario.

It is of note that there exist many other physical mechanisms that can originate a low-temperature anomaly in the electrical resistivity with $d\rho/dT < 0$. For instance it is well known that in disordered systems, quantum interference phenomena can lead to a $\sqrt{T}$ increase in the electrical conductivity, i.e., weak localization. Moreover, as demonstrated recently for stoichiometric Fe_2VAl itself, the conduction mechanism within localized impurity bands arising from intrinsic antisite disorder, may follow a Mott-type variable-range-hopping behavior $\rho(T) \propto \exp(T^{-1/4})$, which will be modified in the presence of strong electronic correlations to $\rho(T) \propto \exp(T^{-1/2})$ (called Efros-Shklovskii hopping). Supplemental Material Fig. S1 shows that, whereas Kondo-type scattering indeed fits the measured data best, the upturn at low temperatures can also qualitatively be described by several of the above-mentioned physical scenarios. Thus, an unambiguous and definite statement about the origin of low-temperature transport anomalies in $Fe_{2-x}Cr_xVAl$ is not feasible.

However, the anomaly of the Seebeck coefficient, the negative magnetoresistance as well as the suggestion of magnetic impurities by DFT-based calculations are consistent with the Kondo-like magnetic scattering.

V. CONCLUSION

XRD crystal structure studies of the compounds $Fe_{2-x}Cr_xVAl$ revealed a high solubility of Cr in Fe_2VAl. The temperature and Cr concentration dependency of both the electrical resistivity and the Seebeck coefficient can be well described taking into account a phenomenological valence electron count of 7 instead of 6. The resulting VEC dependence of the Seebeck is in very good agreement with other studies of p-type doping of Fe_2VAl and hints at the fact that the otherwise non-rigid-band-like Fe/Cr substitution can be phenomenologically compared to an almost rigid-band-like shift of the Fermi level with Cr acting as a p-type doping agent effectively donating one electron per Cr atom.

The low-temperature ($T < 30$-K) properties of $Fe_{2-x}Cr_xVAl$, i.e., a negative logarithmic contribution to the electrical resistivity, the negative magnetoresistance, as well as a minimum in the Seebeck coefficient can be well described by incoherent Kondo scattering of conduction electrons.

The ability to predict changes in the effective VEC for maximizing the thermoelectric performance is an invaluable tool when designing thermoelectric materials for practical application, and Cr substitution has shown to be a well understood and easy to utilize system and certainly will be effective in designing further Fe_2VAl based compounds.

ACKNOWLEDGMENTS

This paper was partially financed by the Japan Science and Technology Agency (JST) Program MIRAI, JPMJMI19A1. For providing their computational capabilities we thank the Vienna Scientific Cluster (VSC) [23].

[1] L. E. Bell, Cooling, heating, generating power, and recovering waste heat with thermoelectric systems, Science **321**, 1457 (2008).

[2] W. Sun, R. Sui, G. Yuan, H. Zheng, Z. Zeng, P. Xie, L. Yuan, Z. Ren, F. Cai, and Q. Zhang, Thermoelectric module design to improve lifetime and output power density, Mater. Today Phys. **18**, 100391 (2021).

[3] Z. Liu, W. Gao, H. Oshima, K. Nagase, C.-H. Lee, and T. Mori, Maximizing the performance of N-type Mg_3Bi_2 based materials for room-temperature power generation and thermoelectric cooling, Nat. Commun. **13**, 1120 (2022).

[4] N. Tsujii, A. Nishide, J. Hayakawa, and T. Mori, Observation of enhanced thermopower due to spin fluctuation in weak itinerant ferromagnet, Sci. Adv. **5**, eaat5935 (2019).

[5] F. Garmroudi, M. Parzer, A. Riss, A. V. Ruban, S. Khmelevskyi, M. Reticcioli, M. Knopf, H. Michor, A. Pustogow, T. Mori *et al.*, Anderson transition in stoichiometric Fe_2VAl: high thermoelectric performance from impurity bands, Nat. Commun. **13**, 1 (2022).

[6] E. Alleno, Review of the thermoelectric properties in nanostructured Fe_2VAl, Metals **8**, 864 (2018).

[7] A. Berche, M. T. Noutack, M.-L. Doublet, and P. Jund, Unexpected band gap increase in the Fe_2VAl Heusler compound, Mater. Today Phys. **13**, 100203 (2020).

[8] F. Garmroudi, M. Parzer, A. Riss, N. Reumann, B. Hinterleitner, K. Tobita, Y. Katsura, K. Kimura, T. Mori, and E. Bauer, Solubility limit and annealing effects on the microstructure & thermoelectric properties of $Fe_2V_{1-x}Ta_xAl_{1-y}Si_y$ Heusler compounds, Acta Mater. **212**, 116867 (2021).

[9] Y. Nishino, S. Deguchi, and U. Mizutani, Thermal and transport properties of the Heusler-type $Fe_2VAl_{1-x}Ge_x(0 \leqslant x \leqslant 0.20)$ alloys: Effect of doping on lattice thermal conductivity, electrical resistivity, and Seebeck coefficient, Phys. Rev. B **74**, 115115 (2006).

[10] B. Hinterleitner, F. Garmroudi, N. Reumann, T. Mori, E. Bauer, and R. Podloucky, The electronic pseudo band gap states and electronic transport of the full-Heusler compound Fe_2VAl, J. Mater. Chem. C **9**, 2073 (2021).

[11] M. Mikami, Y. Kinemuchi, K. Ozaki, Y. Terazawa, and T. Takeuchi, Thermoelectric properties of tungsten-substituted Heusler Fe_2VAl alloy, J. Appl. Phys. **111**, 093710 (2012).

[12] F. Garmroudi, A. Riss, M. Parzer, N. Reumann, H. Müller, E. Bauer, S. Khmelevskyi, R. Podloucky, T. Mori, K. Tobita *et al.*, Boosting the thermoelectric performance of Fe_2VAl-type Heusler compounds by band engineering, Phys. Rev. B **103**, 085202 (2021).

[13] M. Parzer, F. Garmroudi, A. Riss, S. Khmelevskyi, T. Mori, and E. Bauer, High solubility of al and enhanced thermoelectric performance due to resonant states in Fe_2VAl_x, Appl. Phys. Lett. **120**, 071901 (2022).

[14] D. I. Bilc and P. Ghosez, Electronic and thermoelectric properties of Fe_2VAl: the role of defects and disorder, Phys. Rev. B **83**, 205204 (2011).

[15] Y. Feng, J. Y. Rhee, T. A. Wiener, D. W. Lynch, B. E. Hubbard, A. J. Sievers, D. L. Schlagel, T. A. Lograsso, and L. L. Miller, Physical properties of Heusler-like Fe_2VAl, Phys. Rev. B **63**, 165109 (2001).

[16] M. Vasundhara, V. Srinivas, and V. V. Rao, Evidence for cluster glass behavior in Fe_2VAl Heusler alloys, Phys. Rev. B **78**, 064401 (2008).

[17] C. S. Lue, J. H. Ross, Jr, C. F. Chang, and H. D. Yang, Field-dependent specific heat in Fe_2VAl and the question of possible $3d$ heavy fermion behavior, Phys. Rev. B **60**, R13941(R) (1999).

[18] C.-S. Lue, J. H. Ross Jr, K. Rathnayaka, D. Naugle, S. Wu, and W. Li, Superparamagnetism and magnetic defects in Fe_2VAl and Fe_2VGa, J. Phys.: Condens. Matter **13**, 1585 (2001).

[19] J. D. Jong, Thermopower measurements in magnetic fields up to 17 Tesla using the toggled heating method, Rev. Sci. Instrum. **67**, 1970 (1996).

[20] J. Callaway, Model for lattice thermal conductivity at low temperatures, Phys. Rev. **113**, 1046 (1959).

[21] A. Pope, B. Zawilski, and T. Tritt, Description of removable sample mount apparatus for rapid thermal conductivity measurements, Cryogenics **41**, 725 (2001).

[22] B. Hinterleitner, P. Fuchs, J. Rehak, F. Garmroudi, M. Parzer, M. Waas, R. Svagera, S. Steiner, M. Kishimoto, R. Moser *et al.*, Stoichiometric and off-stoichiometric full Heusler $Fe_2V_{1-x}W_xAl$ thermoelectric systems, Phys. Rev. B **102**, 075117 (2020).

[23] See Supplemental Material at http://link.aps.org/supplemental/10.1103/PhysRevB.106.235138 for further details concerning Hall measurements, fitting procedure, various measurements for Si-Cr cosubstituted samples, and further details, such as power factor.

[24] S. Bandaru and P. Jund, Electronic structure of the Heusler compound Fe_2VAl and its point defects by *ab initio* calculations, Phys. Status Solidi B **254**, 1600441 (2017).

[25] J. P. Heremans, B. Wiendlocha, and A. M. Chamoire, Resonant levels in bulk thermoelectric semiconductors, Energy & Environmental Science **5**, 5510 (2012).

[26] T. Graf, C. Felser, and S. S. Parkin, Simple rules for the understanding of Heusler compounds, Prog. Solid State Chem. **39**, 1 (2011).

[27] P. Klemens, Thermal resistance due to point defects at high temperatures, Phys. Rev. **119**, 507 (1960).

[28] S. Anand, R. Gurunathan, T. Soldi, L. Borgsmiller, R. Orenstein, and G. J. Snyder, Thermoelectric transport of semiconductor full-Heusler VFe_2Al, J. Mater. Chem. C **8**, 10174 (2020).

[29] H. Kato, M. Kato, Y. Nishino, U. Mizutani, and S. Asano, Effect of silicon substitution on thermoelectric properties of Heusler-type Fe_2VAl alloy, Nippon Kinzoku Gakkaishi (1952) **65**, 652 (2001).

[30] M. Vasundhara, V. Srinivas, and V. Rao, Low-temperature electrical transport in Heusler-type $Fe_2V(AlSi)$ alloys, J. Phys.: Condens. Matter **17**, 6025 (2005).

[31] C. S. Lue, C. F. Chen, J. Y. Lin, Y. T. Yu, and Y. K. Kuo, Thermoelectric properties of quaternary Heusler alloys $Fe_2VAl_{1-x}Si_x$, Phys. Rev. B **75**, 064204 (2007).

[32] M. Vasundhara, V. Srinivas, and V. V. Rao, Electronic transport in Heusler-type Fe_2VAl_{1-x} M_x alloys (M=B, In, Si), Phys. Rev. B **77**, 224415 (2008).

[33] Y. Terazawa, M. Mikami, T. Itoh, and T. Takeuchi, Effects of heavy element substitution on electronic structure and lattice thermal conductivity of Fe_2VAl thermoelectric material, J. Electron. Mater. **41**, 1348 (2012).

[34] B. Hinterleitner, I. Knapp, M. Poneder, Y. Shi, H. Müller, G. Eguchi, C. Eisenmenger-Sittner, M. Stöger-Pollach, Y. Kakefuda, N. Kawamoto *et al.*, Thermoelectric performance of

a metastable thin-film Heusler alloy, Nature (London) **576**, 85 (2019).

[35] E. J. Skoug, C. Zhou, Y. Pei, and D. T. Morelli, High thermoelectric power factor near room temperature in full-Heusler alloys, J. Electron. Mater. **38**, 1221 (2009).

[36] Y. Nishino, Development of thermoelectric materials based on fe_2val Heusler compound for energy harvesting applications, in *IOP Conference Series: Materials Science and Engineering*, (IOP Publishing, 2011), Vol. 18, p. 142001.

[37] M. Mikami, K. Ozaki, H. Takazawa, A. Yamamoto, Y. Terazawa, and T. Takeuchi, Effect of Ti substitution on thermoelectric properties of W-doped Heusler Fe_2VAl alloy, J. Electron. Mater. **42**, 1801 (2013).

[38] H. Nakayama, N. Ide, and Y. Nishino, Thermoelectric properties of p-type Heusler compounds $(Fe_{2-x}Co_x)(V_{1-y}Ti_y)Al$, Mater. Trans. **49**, 1858 (2008).

[39] Y. Sandaiji, N. Ide, Y. Nishino, T. Ohwada, S. Harada, and K. Soda, Off-stoichiometric effects on thermoelectric properties of Fe_2VAl-based compounds, Funtai Oyobi Funmatsuyakin **57**, 207 (2010).

[40] W. Lu, W. Zhang, and L. Chen, Thermoelectric properties of $(Fe_{1-x}Co_x)_2VAl$ Heusler-type compounds, J. Alloys Compd. **484**, 812 (2009).

[41] J. Kondo, Resistance minimum in dilute magnetic alloys, Prog. Theor. Phys. **32**, 37 (1964).

[42] S. Maekawa, S.-i. Kashiba, M. Tachiki, and S. Takahashi, Thermopower in Ce Kondo systems, J. Phys. Soc. Jpn. **55**, 3194 (1986).

[43] K. H. Fischer, Thermopower of Dilute Magnetic Alloys, *Thermoelectricity in Metallic Conductors*, edited by F. J. Blatt and P. A. Schroeder (Springer, Boston, MA, 1978), pp. 295–305.

[44] J. D. Jong, Thermopower measurements in magnetic fields up to 17 Tesla using the toggled heating method, thesis (1974).

[45] F. J. Blatt and P. A. Schroeder, *Thermoelectricity in Metallic Conductors* (Springer, Berlin, 1978), p. 295.

[46] A. Kowalczyk, V. Tran, T. Toliński, and W. Miiller, Electrical resistivity and thermoelectric power of the Kondo lattice $CeNiAl_4$, Solid State Commun. **144**, 185 (2007).